

Geometric properties of the Fortuin-Kasteleyn representation of the Ising model

Pengcheng Hou,¹ Sheng Fang,¹ Junfeng Wang,^{2,*} Hao Hu,^{3,†} and Youjin Deng^{1,4,‡}

¹*Hefei National Laboratory for Physical Sciences at Microscale and Department of Modern Physics, University of Science and Technology of China, Hefei, Anhui 230026, China*

²*School of Electronic Science and Applied Physics, Hefei University of Technology, Hefei, Anhui 230009, China*

³*School of Physics and Materials Science, Anhui University, Hefei 230601, China*

⁴*CAS Center for Excellence and Synergetic Innovation Center in Quantum Information and Quantum Physics, University of Science and Technology of China, Hefei, Anhui 230026, China*

(Dated: November 9, 2018)

We present a Monte Carlo study of the Fortuin-Kasteleyn (FK) clusters of the Ising model on the square (2D) and simple-cubic (3D) lattices. The wrapping probability, a dimensionless quantity characterizing the topology of the FK clusters on a torus, is found to suffer from smaller finite-size corrections than the well-known Binder ratio, and yields a high-precision critical coupling as $K_c(3D) = 0.221\,654\,631(8)$. We then study geometric properties of the FK clusters at criticality. It is demonstrated that the distribution of the critical largest-cluster size C_1 follows a single-variable function as $P(C_1, L)dC_1 = \tilde{P}(x)dx$ with $x \equiv C_1/L^{d_F}$ (L is the linear size), and that the fractal dimension d_F is identical to the magnetic exponent. An interesting bimodal feature is observed in distribution $\tilde{P}(x)$ in 3D, and attributed to the different approaching behaviors for $K \rightarrow K_c + 0^\pm$. For a critical FK configuration, the cluster number per site $n(s, L)$ of size s is confirmed to obey the standard scaling form $n(s, L) \sim s^{-\tau} \tilde{n}(s/L^{d_F})$, with hyper-scaling relation $\tau = 1 + d/d_F$ and the spatial dimension d . To further characterize the compactness of the FK clusters, we measure their graph distances and determine the shortest-path exponents as $d_{\min}(3D) = 1.259\,4(2)$ and $d_{\min}(2D) = 1.094\,0(3)$. Further, by excluding all the bridges from the occupied bonds, we obtain bridge-free configurations and determine the backbone exponents as $d_B(3D) = 2.167\,3(15)$ and $d_B(2D) = 1.732\,1(4)$. The estimates of the universal wrapping probabilities for the 3D Ising model and of the geometric critical exponents d_{\min} and d_B either improve over the existing results or have not been reported yet.

PACS numbers: 05.50.+q, 05.70.Jk, 64.60.F-

I. INTRODUCTION

The Ising model [1] plays an important role in the study of phase transitions and critical phenomena. The model exhibits finite-temperature phase transitions in two and more dimensions. It can be solved exactly for a few two-dimensional lattices [2, 3], leading to exact values of phase transition points and critical exponents, which are very often used as benchmarks for new theories and methods. In three dimensions, since an exact solution of the Ising model is still unavailable, one usually applies approximation methods or numerical simulations [4], among which the Monte Carlo (MC) method is probably one of the best.

Most studies of the Ising model focus on the thermodynamic properties. Quantities of interest include the magnetization, susceptibility, energy, heat capacity, and spin-spin correlations etc. Under the Fortuin-Kasteleyn (FK) transformation [5], the partition sum of the Ising model can be written as summation over random cluster configurations. The FK representation is a key ingre-

dent of the Swendsen-Wang algorithm [6, 7], in which non-local updates make the algorithm significantly suppress critical slowing-down. As geometric objects, the FK clusters also exhibit critical behaviors near the phase transition point. An example is the wrapping probability [8–10], which is defined as the probability that there exists a cluster which wraps around the periodic boundaries of a finite lattice. This quantity takes a universal value at criticality [8, 9, 11], and has also been proven to be a good choice in estimating the critical temperature for continuous phase transitions due to its impressively small leading finite-size corrections [12, 13],

In this paper, we conduct a Monte Carlo study of the FK clusters of the Ising model on the square (2D) and simple-cubic (3D) lattices. By performing finite-size scaling (FSS) analysis of the wrapping probabilities, we obtain a high-precision estimate of the critical coupling for the 3D Ising model as $K_c = 0.221\,654\,631(8)$. This provides an independent check of the most recent result $K_c = 0.221\,654\,626(5)$ in Ref. [4], in which a state-of-the-art method, making use of cross correlations, is applied to reduce statistical errors and extensive simulations were carried out up to an impressive linear size $L = 1024$. The universal values of the wrapping probabilities for the 3D Ising model are determined, which have not been reported yet.

Geometric properties of the critical FK clusters are

*Electronic address: wangjf@hfut.edu.cn

†Electronic address: huhao@ahu.edu.cn

‡Electronic address: yjdeng@ustc.edu.cn

studied. The probability distribution of the critical largest-cluster size C_1 is found to obey a single-variable function as $P(C_1, L)dC_1 = \tilde{P}(x)dx$ with $x \equiv C_1/L^{d_F}$, where the fractal dimension d_F is identical to the magnetic renormalization exponent y_h . The function $\tilde{P}(x)$ displays a clear bimodal feature in 3D, while in 2D, it exhibits an asymmetric peak with a shoulder shape at the smaller- x side. By fine-tuning simulations at L -dependent coupling $K \rightarrow K_c + 0^\pm$, we find that the two modes correspond to the distinct asymptotic behaviors approaching from the low- and high-temperature sides. Then, we consider full FK configurations and measure the cluster number per site $n(s, L)$ of size s . As expected, the standard scaling $n(s, L) \sim s^{-\tau} \tilde{n}(s/L^{d_F})$ is observed both in 2D and 3D, and the hyper-scaling relation $\tau = 1 + d/d_F$ is well satisfied (d is the spatial dimension). To characterize the compactness of the FK clusters, we record their graph distances and determine the shortest-path exponents as $d_{\min}(3D) = 1.2594(2)$ and $d_{\min}(2D) = 1.0940(3)$. In addition, we classify the occupied bonds into bridges and non-bridges; an occupied bond is a bridge iff its deletion leads to the breaking of a FK cluster. By excluding all the bridges, we obtain bridge-free configurations and determine the backbone exponents as $d_B(3D) = 2.1673(15)$ and $d_B(2D) = 1.7321(4)$. These estimates of d_{\min} and d_B either improve over the existing results or have not been reported yet, to our knowledge.

The remainder of this paper is organized as follows. Section II describes the model, simulation and sampled quantities. Section III presents the results for the wrapping probabilities of the FK clusters, and the estimate of the critical coupling K_c for the 3D Ising model. Section IV studies other geometric properties of the FK clusters, including the probability distribution of the largest-cluster size, the cluster number per site $n(s, L)$, the graph distances of the FK clusters, the size of the largest cluster in the bridge-free configuration, and the thermodynamic bond densities of various types. A brief summary and discussion is given in Sec. V. The Appendix collects results on other observables for the Ising model.

II. MODEL, SIMULATION AND SAMPLED QUANTITIES

A. Model

We simulate the spin-1/2 Ising model on the $L \times L$ square and $L \times L \times L$ simple-cubic lattices with periodic boundary conditions, where L is the linear extent. The spin-1/2 Ising model with a vanishing external field is defined by the Hamiltonian

$$H/k_B T = -K \sum_{\langle \mathbf{x}\mathbf{y} \rangle} \sigma_{\mathbf{x}} \sigma_{\mathbf{y}} \quad , \quad (1)$$

where the spins assume values $\sigma_{\mathbf{x}} \in \{-1, 1\}$, and $\mathbf{x} = (x_0, x_1)$ or (x_0, x_1, x_2) denotes a vertex with $x_i \in$

$\{1, 2, \dots, L\}$, $\langle \mathbf{x}\mathbf{y} \rangle$ sums over all the pairs of nearest neighbors on the lattice. Symbols T , k_B , K represent the physical temperature, the Boltzmann constant and the reduced coupling, respectively. In the FK transformation [5], for a given lattice \mathcal{G} with edge set $\{\langle \mathbf{x}\mathbf{y} \rangle\}$, the clusters are formed by putting a bond on each edge with probability $p = (1 - e^{-2K})\delta_{\sigma_{\mathbf{x}}\sigma_{\mathbf{y}}}$. A cluster is defined as a connected component consisting of vertices and bonds. Then the partition function can be written as

$$Z_{\text{RC}}(v) = \sum_{\mathcal{A} \subseteq \mathcal{G}} v^{\mathcal{N}_{\text{bond}}} q^{\mathcal{N}_c} \quad , \quad (v = e^{2K} - 1) \quad (2)$$

where q accounts for the statistical weight for each FK cluster, $\mathcal{N}_{\text{bond}}$ and \mathcal{N}_c are the number of occupied bonds and clusters, respectively. The summation is over all subgraphs \mathcal{A} of the lattice \mathcal{G} . The system is referred to be the random-cluster (RC) model. The Ising model has $q = 2$.

B. Simulation and sampled quantities

In simulating the Ising model, we employ the Wolff cluster flipping algorithm [14] and the Swendsen-Wang algorithm [6]. The latter is used to generate FK clusters over the whole lattice. The occupied bonds on a complete FK configuration can be classified into bridges and non-bridges [15, 16]. A bridge bond is an occupied bond whose deletion would break a cluster. We delete all bridges to produce a bridge-free configuration. The corresponding processes are described in Ref. [15, 16], which we skip hereby. Our simulation in 3D is up to $L = 512$. For $L = 512, 384, 256$ and 192 , the numbers of samples are about 4×10^6 , 1.5×10^7 , 1.3×10^8 and 1.3×10^8 , respectively. For each $L \leq 128$, no less than 5×10^8 samples are generated. The 2D simulation is up to $L = 1024$. The numbers of samples are about 3.6×10^6 and 10^7 for $L = 1024$ and 768 , respectively, no less than 2×10^7 samples for $L = 512, 384, 256, 192, 128$ and 96 , and around 10^8 for each $L \leq 64$. For a configuration, we sample the following observables:

- The indicators $\mathcal{R}^{(x)}$, $\mathcal{R}^{(y)}$, and $\mathcal{R}^{(z)}$, for the event that a cluster wraps around the lattice in the x , y , or z directions, respectively.
- The size of the largest cluster \mathcal{C}_1 .
- The size of the largest cluster on the bridge-free configuration $\mathcal{C}_{1,\text{bf}}$.
- An observable $\mathcal{S} := \max_C \max_{y \in C} d(x_C, y)$ is used to determine the shortest-path exponent. Here $d(x, y)$ denotes the graph distance from vertex x to vertex y , and x_C is the vertex in cluster C with the smallest vertex label, according to some fixed (but arbitrary) vertex labeling.

- The numbers \mathcal{N}_b , \mathcal{N}_j , \mathcal{N}_n of branch, junction and non-bridge bonds, respectively. The bridge bond is a junction bond if neither of the two resulting clusters is a tree; otherwise, it is a branch bond [15, 16].
- The square \mathcal{M}^2 and the fourth power \mathcal{M}^4 of the magnetization density \mathcal{M} , where \mathcal{M} is defined as $\mathcal{M} = \frac{1}{L^d} \sum_x \sigma_x$ with d the spatial dimension.

From these observables we calculate the following quantities:

- The wrapping probabilities

$$\begin{aligned} R^{(x)} &= \langle \mathcal{R}^{(x)} \rangle = \langle \mathcal{R}^{(y)} \rangle = \langle \mathcal{R}^{(z)} \rangle, \\ R^{(2)} &= \langle \mathcal{R}^{(x)} \mathcal{R}^{(y)} \rangle = \langle \mathcal{R}^{(x)} \mathcal{R}^{(z)} \rangle = \langle \mathcal{R}^{(y)} \mathcal{R}^{(z)} \rangle, \\ R^{(3)} &= \langle \mathcal{R}^{(x)} \mathcal{R}^{(y)} \mathcal{R}^{(z)} \rangle. \end{aligned} \quad (3)$$

Here $R^{(x)}$, $R^{(2)}$ and $R^{(3)}$ give the probabilities that a winding exists in the x direction, in two of the three possible directions, and simultaneously in the three directions, respectively. At K_c , these wrapping probabilities take non-zero universal values in the thermodynamic limit $L \rightarrow \infty$.

- The mean size of the largest cluster $C_1 = \langle \mathcal{C}_1 \rangle$, which scales as $C_1 \sim L^{d_F}$ at K_c , with d_F the fractal dimension of the FK clusters.
- The mean size of the largest cluster $C_{1,\text{bf}} = \langle \mathcal{C}_{1,\text{bf}} \rangle$ in the bridge-free configuration, which scales as $C_{1,\text{bf}} \sim L^{d_B}$ at K_c , with d_B the backbone dimension.
- The mean shortest-path distance $S = \langle \mathcal{S} \rangle$, which scales $S \sim L^{d_{\text{min}}}$ at K_c , with d_{min} the shortest-path fractal dimension.
- The number densities $\rho_b = \langle \mathcal{N}_b \rangle / L^d$, $\rho_j = \langle \mathcal{N}_j \rangle / V$ and $\rho_n = \langle \mathcal{N}_n \rangle / V$ of the branch, junction and non-bridge bonds, respectively. The leading scaling terms of these bond densities are proportional to L^{y_t-d} .

- The Binder cumulant

$$Q_m = \frac{\langle \mathcal{M}^4 \rangle}{\langle \mathcal{M}^2 \rangle^2}, \quad (4)$$

In addition, we record the statistics of the cluster number per site $n(s, L)$ of size s , and the probability distribution $P(C_1, L) dC_1$ for the largest-cluster size C_1 .

For computational efficiency, we use standard reweighting method [17] to obtain the expectations of the wrapping probabilities and the Binder cumulant for multiple values of K around K_c .

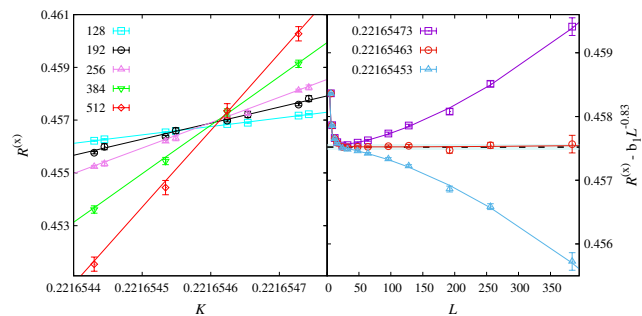


FIG. 1: Plots of $R^{(x)}$ vs K for different system sizes L (left) and $R^{(x)}(K, L) - b_1 L^{-0.83}$ vs L for fixed values of K (right) for the 3D Ising model. The value of b_1 is taken from Table I.

III. WRAPPING PROBABILITIES AND CRITICAL POINT IN 3D

The wrapping probability is a universal geometric quantity which reflects topological properties of the system under study. This quantity was first introduced for percolation [8]. Later, analytical results of various wrapping probabilities of percolation clusters on the 2D torus were derived by Pinson [9], built on works of Nienhuis [18], di Francesco et al. [19], and Cardy [20]. Arguin extended Pinson's work to the case of 2D RC models with $1 \leq q \leq 4$ and derived the closed forms of wrapping probabilities in terms of Jacobi θ functions [10]. Finite-size corrections of wrapping probabilities for the RC model in the canonical ensemble (where the total number of the occupied bonds is fixed) were also studied recently [21]. In 3D, there also exist a few studies on the wrapping probabilities [13, 22]. Nevertheless, no results concerning the wrapping probability of the FK clusters for the 3D Ising model have been reported.

In numerical studies of phase transitions, dimensionless quantities like the Binder cumulant Q_m are known to provide powerful tools for locating critical points. The wrapping probabilities, topological and dimensionless quantities, should also provide a useful method for estimating K_c . This is demonstrated in the left plot of Fig. 1 for the 3D Ising model. The intersections of the $R^{(x)}$ data for different system sizes L would give the critical couplings $K_c \approx 0.221\,654\,6$, with an uncertainty at the seventh decimal place.

In order to estimate K_c more accurately, we resort to the fitting of the data. Around K_c , we perform least-squares fits of the MC data for the wrapping probabilities $R^{(x)}$, $R^{(2)}$, $R^{(3)}$ and the Binder cumulant Q_m by the ansatz

$$\begin{aligned} \mathcal{O}(\epsilon, L) &= \mathcal{O}_c + \sum_{k=1}^2 q_k \epsilon^k L^{k y_t} + c_1 \epsilon L^{y_t + y_i} \\ &\quad + b_1 L^{y_i} + b_2 L^{-2} + b_3 L^{-3}, \end{aligned} \quad (5)$$

where $\epsilon = K_c - K$, \mathcal{O}_c is a universal constant, y_t is the thermal scaling exponent and y_i is the leading correction exponent.

TABLE I: Fits of the wrapping probabilities $R^{(x)}, R^{(2)}, R^{(3)}$ and the Binder cumulant Q_m for the 3D Ising model. ‘Obs.’ is the abbreviation of the phrase ‘observables’.

Obs.	L_{\min}	χ^2/DF	K_c	y_t	\mathcal{O}_c	q_1	b_1	y_i	b_2	b_3
$R^{(x)}$	12	86.1/156	0.221 654 633(3)	1.60(2)	0.457 59(4)	-1.4(1)	-0.036(2)	-0.80(2)	0.009(9)	-
	16	75.7/140	0.221 654 631(4)	1.59(2)	0.457 53(6)	-1.4(1)	-0.040(5)	-0.84(4)	0.04(3)	-
	24	71.5/124	0.221 654 629(4)	1.59(2)	0.457 49(9)	-1.4(2)	-0.05(2)	-0.88(8)	0.08(8)	-
	12	89.4/157	0.221 654 629(2)	1.60(2)	0.457 529(7)	-1.38(10)	-0.038 9(2)	-0.83	0.024(2)	-
	16	75.8/141	0.221 654 631(2)	1.59(2)	0.457 54(1)	-1.4(2)	-0.039 3(3)	-0.83	0.032(4)	-
	24	72.0/125	0.221 654 631(3)	1.59(2)	0.457 55(2)	-1.4(2)	-0.039 4(5)	-0.83	0.03(2)	-
$R^{(2)}$	12	91.9/134	0.221 654 633(3)	1.60(2)	0.332 01(4)	-1.3(1)	-0.093(3)	-0.874(9)	-0.25(1)	-
	16	73.8/121	0.221 654 629(4)	1.59(2)	0.331 93(6)	-1.4(1)	-0.101(6)	-0.90(2)	-0.21(3)	-
	24	71.2/108	0.221 654 628(4)	1.59(2)	0.331 90(9)	-1.4(2)	-0.11(2)	-0.92(4)	-0.17(9)	-
	12	98.6/134	0.221 654 637(3)	1.60(2)	0.332 12(2)	-1.3(1)	-0.080 3(5)	-0.83	-0.37(2)	0.45(11)
	16	75.9/121	0.221 654 633(3)	1.59(2)	0.332 07(3)	-1.4(2)	-0.078(1)	-0.83	-0.47(5)	1.5(4)
	24	72.1/108	0.221 654 631(4)	1.59(2)	0.332 04(4)	-1.4(2)	-0.076(2)	-0.83	-0.6(2)	3(2)
$R^{(3)}$	12	110.4/134	0.221 654 634(3)	1.60(2)	0.267 25(4)	-1.3(1)	-0.117(3)	-0.885(8)	-0.32(2)	-
	16	87.9/121	0.221 654 629(4)	1.59(2)	0.267 14(5)	-1.3(1)	-0.131(7)	-0.92(2)	-0.25(3)	-
	24	85.9/108	0.221 654 629(5)	1.59(2)	0.267 13(9)	-1.3(2)	-0.13(2)	-0.92(4)	-0.24(9)	-
	16	86.0/135	0.221 654 635(3)	1.59(2)	0.267 34(3)	-1.3(2)	-0.094(1)	-0.83	-0.66(5)	2.3(4)
	24	80.1/122	0.221 654 633(4)	1.59(2)	0.267 30(4)	-1.3(2)	-0.092(2)	-0.83	-0.8(2)	4(2)
	32	76.6/109	0.221 654 628(5)	1.58(2)	0.267 19(8)	-1.4(2)	-0.085(5)	-0.83	-1.5(5)	16(8)
Q_m	12	83.3/135	0.221 654 623(4)	1.59(2)	1.603 53(8)	2.1(2)	-0.271(5)	-0.860(7)	-0.25(3)	-
	16	80.9/122	0.221 654 624(5)	1.59(2)	1.603 5(2)	2.1(3)	-0.276(10)	-0.87(2)	-0.22(6)	-
	24	77.5/109	0.221 654 623(6)	1.59(2)	1.603 6(2)	2.1(3)	-0.27(3)	-0.85(3)	-0.3(2)	-
	12	86.0/135	0.221 654 617(3)	1.59(2)	1.603 76(3)	2.1(3)	-0.245(1)	-0.83	-0.55(2)	1.0(3)
	16	80.1/122	0.221 654 621(4)	1.59(2)	1.603 68(5)	2.1(3)	-0.241(2)	-0.83	-0.49(4)	2.5(8)
	24	76.6/109	0.221 654 622(5)	1.59(2)	1.603 65(8)	2.1(3)	-0.239(4)	-0.83	-0.65(9)	4(3)

As a precaution against correction-to-scaling terms that we have neglected in our chosen ansatz, we impose a lower cutoff $L \geq L_{\min}$ on the data points admitted in the fit, and systematically study the effect on the χ^2 value when L_{\min} is increased. In general, our preferred fit for any given ansatz corresponds to the smallest L_{\min} for which χ^2 divided by the number of degrees of freedom (DFs) is $O(1)$, and for which subsequent increases in L_{\min} do not cause χ^2 to drop by much more than one unit per degree of freedom. In the fits with y_i free and $b_3 = 0$ fixed, our results of y_i estimated from $R^{(x)}$ is consistent with $y_i \approx -0.83$, as determined elsewhere [23, 24]. In the subsequent fits, we fix $y_i = -0.83$ for all quantities since in theory y_i should be a universal correction exponent. In most cases, when performing the fits with y_i fixed, we include the correction term $b_3 L^{-3}$. However, for $R^{(x)}$ when leave b_3 free it can not be determined, and thus we only use $b_1 L^{-0.83} + b_2 L^{-2}$ as correction terms. Table I summarizes the fitting results.

From Table I we observe that in comparison with Q_m , the wrapping probabilities, especially $R^{(x)}$, clearly have smaller amplitudes of the leading corrections. Due to the weaker corrections, the results of K_c fitted from the wrapping probabilities have relatively smaller error bars. We mention that weaker corrections have also been found for wrapping probabilities in percolation [13]. From $R^{(x)}$, we estimate $K_c = 0.221 654 630(6)$ and $R_c^{(x)} = 0.457 5(1)$. We also obtain K_c and \mathcal{O}_c for other observables. Table I also gives the estimate of the thermal exponent $y_t \approx 1.59$.

After comparing the fits of K_c from various wrapping probabilities, we present our final estimate as $K_c(3\text{D}) = 0.221 654 631(8)$. The right plot of Fig. 1 demonstrates the values of K_c and $R_c^{(x)}$, where $R^{(x)} - b_1 L^{-0.83}$ is plotted versus L . The value of the parameter b_1 is taken from Table I. Precisely at $K = K_c$, the $L \rightarrow \infty$ data tend to a horizontal line, whereas the data with $K \neq K_c$ bend upward or downward.

Our estimate agrees well with the most recent result 0.221 654 626(5) by Ferrenberg et al. [4] within one sigma error bar but with slightly lower precision. Since Ref. [4] used cross correlations to reduce statistical errors and carried out simulations up to an impressive linear size $L = 1024$, our result provides a valuable and independent check. A previous estimate 0.221 654 55(3) [23] reported by one of our authors and his collaborator is also ruled out.

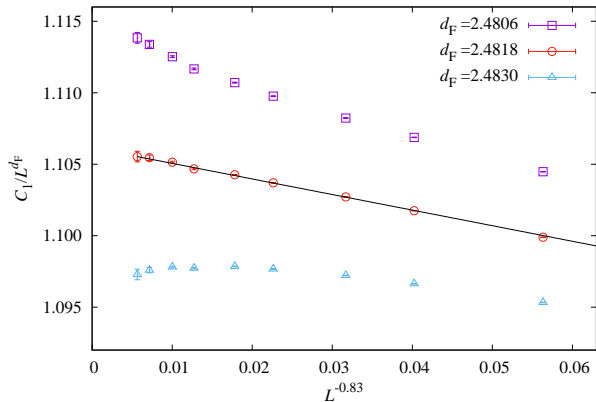
In Appendix A 1, we determine the thermal exponent as $y_t = 1.587 0(5)$ by analyzing the covariance of the wrapping probability and the energy density, which is also consistent with the result 1.587 5(3) in Ref. [4].

IV. GEOMETRICAL PROPERTIES OF FK CLUSTERS AT K_c

Fixing K at our estimated critical coupling 0.221 654 63 for the simple cubic lattice and the exact solution $\ln(1 + \sqrt{2})/2 \approx 0.440 686 79$ for the

TABLE II: Fits of C_1 for the 3D and 2D Ising models.

	L_{\min}	χ^2/DF	d_F	a_0	b_1	y_1	b_2
3D	8	6.2/8	2.4817(3)	1.107(2)	-0.096(10)	-0.78(7)	-0.30(4)
	12	6.2/7	2.4817(4)	1.107(3)	-0.10(3)	-0.79(12)	-0.29(10)
	12	6.3/8	2.48182(6)	1.1060(4)	-0.106(3)	-0.83	-0.25(3)
	16	5.6/7	2.48178(8)	1.1063(5)	-0.109(5)	-0.83	-0.21(5)
	24	5.2/6	2.48184(13)	1.1059(9)	-0.104(9)	-0.83	-0.3(2)
2D	8	14.0/11	1.87501(2)	1.0070(1)	-0.039(7)	-1.6(1)	-
	12	14.0/10	1.87501(3)	1.0070(2)	-0.04(2)	-1.6(3)	-
	16	12.3/9	1.87502(3)	1.0070(2)	-0.12(15)	-2.0(5)	-
	16	12.3/10	1.875024(13)	1.00691(6)	-0.12(1)	-2	-
	24	12.2/9	1.875020(17)	1.00693(8)	-0.13(3)	-2	-

FIG. 2: Plots of C_1/L^{d_F} vs $L^{-0.83}$ for the critical 3D Ising model.

square lattice, we analyze geometrical quantities defined in Sec.II. These include the size of the largest cluster C_1 , the shortest-path distance S , the size of the largest cluster on the bridge-free configuration $C_{1,\text{bf}}$. These analyses allow us estimate the fractal dimension d_F , the shortest-path fractal dimension d_{\min} , the backbone fractal dimension d_B . In addition, we study the cluster-size distribution and the probability distribution of the size of the largest cluster.

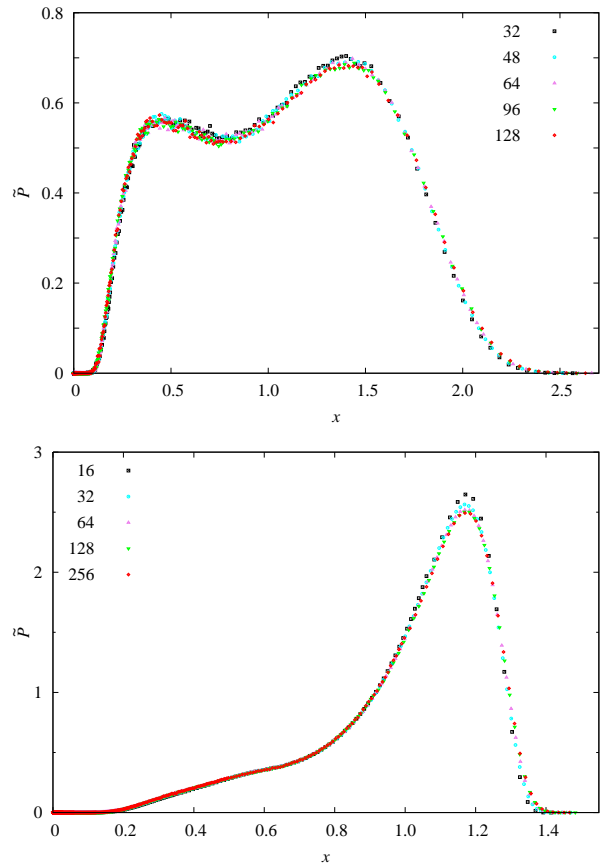
A. Fractal dimension d_F and the probability distribution of the largest-cluster size

In order to estimate d_F , we fit the MC data of C_1 to the following equation d_F ,

$$A = L^{y_A}(a_0 + b_1 L^{y_1} + b_2 L^{y_2}). \quad (6)$$

For the 3D Ising model, when we perform the fit with $y_2 = -2$ fixed and y_1 free, we observe that $y_1 \approx -0.83$. To reduce one fitting parameter, in the subsequent fit we fix $y_1 = -0.83$ and $y_2 = -2$. The fitting results are shown in Table II. We also try the fit using $b_1 L^{-1} + b_2 L^{-2}$ as correction terms for 2D and 3D, in that case b_2 cannot be determined and the corresponding results are not shown in the table.

Comparing these fits, we determine the fractal dimensions $d_F = 2.4818(4)$ for 3D and $1.87501(4)$ for 2D. The

FIG. 3: Probability density distribution of the largest-cluster size for 3D (top) and 2D (bottom) at K_c , with $x \equiv C_1/L^{d_F}$.

latter agrees with the exact value $y_h = 15/8$ [25, 26]. In Fig. 2, we plot C_1/L^{d_F} versus $L^{-0.83}$ using three different values of d_F for the 3D Ising model: namely our estimate, as well as the estimate plus or minus three standard deviations. As L increases, the data with $d_F = 2.4806$ and $d_F = 2.4830$ bend upward and downward, respectively, while the data with $d_F = 2.4818$ are consistent with a straight line. This illustrates the reliability of our estimate.

We also study the probability distribution $P(C_1, L)dC_1$ of the size of the largest cluster C_1 . In the MC simulation, $P(C_1, L)dC_1$ is measured by the fraction of the number of the configurations on which the size of the largest cluster lies between $C_1 \sim C_1 + dC_1$. According to finite-size scaling theory, we expect that $P(C_1, L)dC_1$ can be expressed as a single-variable function $\tilde{P}(x)dx$, with $x \equiv C_1/L^{d_F}$. This is well confirmed by Fig. 3, where the data for different system sizes collapse on top of each other. Interestingly, we see that the scaling function $\tilde{P}(x)$ exhibits a bimodal structure in 3D, and a single peak with a wide shoulder shape in the small- x side in 2D.

To understand the bimodal structure in 3D, we explore $\tilde{P}(x)$ in the critical window $\Delta \equiv L^{y_t}(K - K_c)$, with Δ a

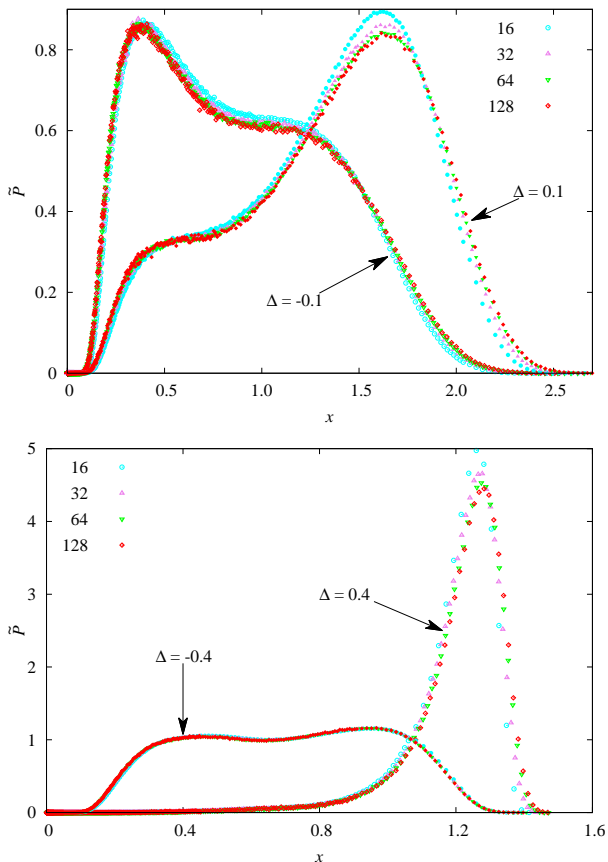


FIG. 4: Probability density distribution of the largest-cluster size for 3D (top) with $K = K_c \pm \Delta L^{-y_t}$ and 2D (bottom) with $K = K_c \pm \Delta L^{-y_t}$.

finite constant. An example with $\Delta = \pm 0.1$ is shown in the top plot of Fig. 4, where the distributions become to have a single peak with a wide shoulder shape. Therefore, it is reasonable to assume that the asymptotical peak locations $x_{\max}(\Delta \rightarrow 0^\pm)$ are actually different. From the similarity between the 3D low-temperature distribution with $\Delta = 0.1$ (the top plot of Fig. 4) and the 2D critical one (the bottom plot of Fig. 3), we expect that a bimodal distribution would appear for 2D in the high-temperature region with $\Delta < 0$. The 2D results with $\Delta = \pm 0.4$ are shown in the bottom plot of Fig. 4, confirming our expectation.

B. Cluster-size distribution

We consider the critical cluster-number density $n(s, L)$ of size s , of which the scaling behavior is expected to follow

$$n(s, L) = s^{-\tau} \tilde{n}(s/L^{d_F}), \quad (7)$$

where $\tau = 1 + d/d_F$ is Fisher exponent and $\tilde{n}(x)$ with $x \equiv s/L^{d_F}$ is a universal scaling function. From $d_F \approx 2.4818$

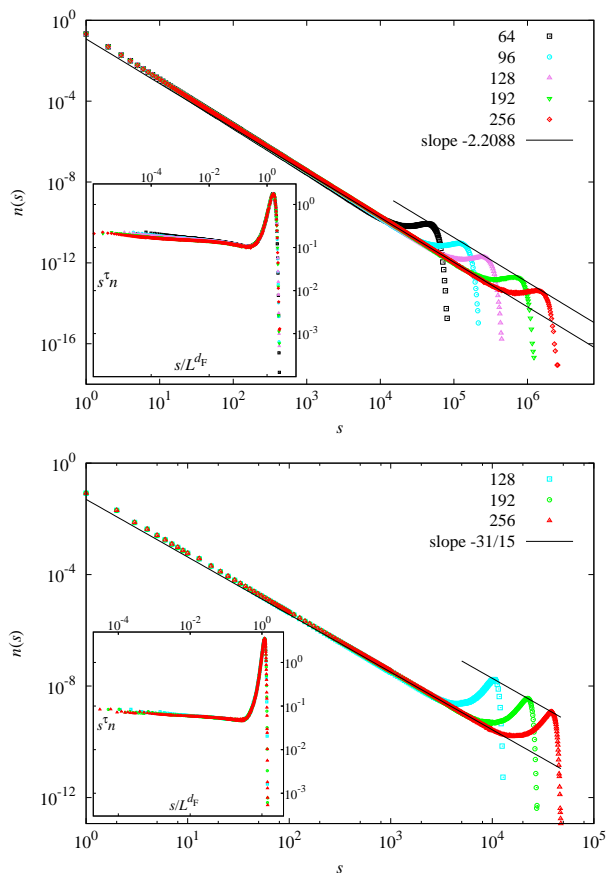


FIG. 5: Cluster-size distribution for FK clusters for 3D (top) and 2D (bottom) at criticality. In both cases, the insets show $s^\tau n(s)$ vs s/L^{d_F} .

(3D) or $15/8$ (2D), one has $\tau \approx 2.2088$ (3D) or $31/15$ (2D), respectively. In the main plots of Fig. 5, we show a log-log plot of $n(s)$ versus s for $L = 64, 96, 128, 192$ and 256 for the 3D Ising model, and for $L = 128, 192$ and 256 for the 2D Ising model. The straight lines with slope -2.2088 (3D) and $31/15$ (2D) are drawn for comparison with the MC data. In these plots, we observe clearly the power-law behaviors $n(s, \infty) \sim s^{-2.2088}$ (3D) and $n(s, \infty) \sim s^{-31/15}$ (2D), respectively.

In order to display the universal scaling function $\tilde{n}(x)$, we further plot $s^{2.2088} n(s, L)$ versus $s/L^{2.4818}$ (3D) and $s^{31/15} n(s, L)$ versus $s/L^{15/8}$ (2D) for several system sizes, and show them in the insets of Fig. 5. We find a good collapse of those curves for different system sizes, which provides strong numerical evidence for the conjectured scaling Eq.(7).

C. Shortest-path fractal dimension d_{\min}

We estimate the shortest-path fractal dimension d_{\min} for the 3D and 2D Ising models by studying the shortest-path distance S . The MC data for S are fitted to Eq. (6) with the exponent y_A being replaced by d_{\min} . For the 3D

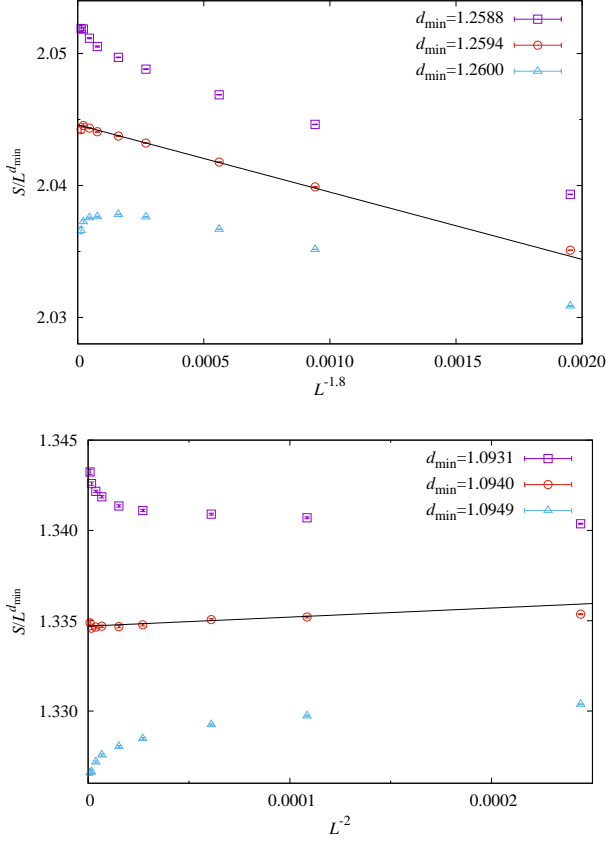


FIG. 6: Plots of $S/L^{d_{\min}}$ vs $L^{-1.8}$ or L^{-2} for the critical 3D (top) or 2D Ising model (bottom), respectively.

Ising model, with $y_2 = -3$ and y_1 being free, we obtain $y_1 = -1.8(2)$, much smaller than $y_i \approx -0.83$ from the leading irrelevant thermal scaling field. On this basis, we further perform the fit with $y_1 = -1.8$ and $y_2 = -3$ fixed. For the 2D Ising model, setting $b_2 = 0$ and y_1 free, y_1 cannot be determined by our MC data. We then try the fit with $y_1 = -2$ fixed and find b_1 consistent with zero. On this basis, we perform the fit with $b_1 = 0$ and $b_2 = 0$. Thus, S suffers rather small finite-size corrections both in 2D and 3D.

From these fits, we estimate $d_{\min} = 1.2594(2)$ (3D) and $1.0940(3)$ (2D), respectively. As far as we know, the shortest-path fractal dimension of the 3D Ising FK clusters has not been estimated. The 2D result improves over the previous reported value $d_{\min} = 1.0955(10)$ [27].

To illustrate our estimate, Fig. 6 shows a plot of $S/L^{d_{\min}}$ versus $L^{-1.8}$ (3D) and a plot of $S/L^{d_{\min}}$ versus L^{-2} (2D) at three different d_{\min} values. In both cases, using the estimated values of d_{\min} produces a straight line, in contrast the other two curves bend upward or downward for large L . The figure suggests that the true value of d_{\min} does indeed lie within 3σ of our estimate.

TABLE III: Fits of S for the 3D and 2D Ising models.

	L_{\min}	χ^2/DF	d_{\min}	a_0	b_1	y_1	b_2
3D	16	9.3/6	1.25934(5)	2.0453(5)	-5.0(8)	-1.78(5)	27(5)
	24	6.2/5	1.25942(6)	2.0443(7)	-9(4)	-1.9(1)	60(24)
	16	9.5/7	1.25936(2)	2.0450(2)	-5.38(4)	-1.8	29.5(7)
	24	8.0/6	1.25934(3)	2.0452(3)	-5.48(9)	-1.8	33(3)
	32	7.0/5	1.25937(4)	2.0449(4)	-5.3(2)	-1.8	25(9)
2D	96	6.7/5	1.09399(6)	1.3347(5)	5(2)	-2	-
	128	2.9/4	1.09409(8)	1.3339(6)	10(3)	-2	-
	192	2.9/3	1.09408(12)	1.334(1)	9(9)	-2	-
	192	4.2/4	1.09396(5)	1.3350(4)	-	-	-
	256	3.0/3	1.09400(6)	1.3347(5)	-	-	-

TABLE IV: Fits of $C_{1,\text{bf}}$ for the 3D and 2D Ising models.

	L_{\min}	χ^2/DF	d_B	a_0	b_1	y_1	b_2
3D	8	8.9/6	2.1680(7)	0.621(3)	0.40(2)	-0.78(3)	-0.50(8)
	12	6.9/5	2.1669(9)	0.626(4)	0.46(6)	-0.85(6)	-0.8(3)
	12	7.0/6	2.1673(2)	0.6242(8)	0.439(6)	-0.83	-0.71(5)
	16	6.0/5	2.1671(3)	0.615(1)	0.433(9)	-0.83	-0.6(1)
	24	4.8/4	2.1674(5)	0.624(2)	0.45(2)	-0.83	-0.9(3)
2D	8	12.7/11	1.73214(13)	0.7997(7)	0.1168(9)	-0.66(2)	-
	12	10.5/10	1.7320(2)	0.8008(10)	0.119(2)	-0.69(2)	-
	16	8.6/9	1.7322(3)	0.7996(14)	0.116(3)	-0.66(3)	-
	8	13.1/12	1.73207(4)	0.8001(2)	0.1172(4)	-0.67	-
	12	11.2/11	1.73210(4)	0.8000(2)	0.1178(6)	-0.67	-
16	8.8/10	1.73206(5)	0.8002(3)	0.1169(9)	-0.67	-	

D. Backbone fractal dimension d_B

In order to estimate the backbone fractal dimension d_B for the 3D and 2D Ising models, we fit the MC data of $C_{1,\text{bf}}$ to Eq.(6) with y_A being replaced by d_B . For the 3D Ising model, in the fit with $y_2 = -2$ fixed and y_1 free, we observe that $y_1 \approx -0.83$. On this basis we fix $y_1 = -0.83$ and $y_2 = -2$. For the 2D Ising model, when set $b_2 = 0$ and leave y_1 free, we find that $y_1 \approx -0.67$, suggesting rather strong finite-size corrections.

The fitting results are shown in Table IV. Comparing these fits, we estimate the backbone fractal dimension as $d_B = 2.1673(15)$ (3D) and $1.7321(4)$ (2D), respectively. The 3D result improves over the previous reported value $d_B(3D) = 2.171(4)$ [28], and the 2D result rules out the previous estimate $d_B(2D) = 1.7304(3)$ [29]. These previous reported values were estimated by studying the scaling behavior of the probability that a pair of lattice sites at a distance r are connected by at least two mutually independent paths. Similarly, by using three different d_B values, in Fig. 7 we plot $C_{1,\text{bf}}/L^{d_B}$ versus $L^{-0.83}$ (3D) or $L^{-0.67}$ (2D), illustrating the reliability of our estimate of d_B .

E. Bond densities ρ_b , ρ_j and ρ_n

In order to estimate the critical bond densities for branch, junction and non-bridge bonds for the 3D and 2D Ising models, we fit the MC data of ρ_b , ρ_j and ρ_n to the ansatz

$$\rho = \rho_0 + L^{y_t-d}(a + bL^{y_1}) \quad (8)$$

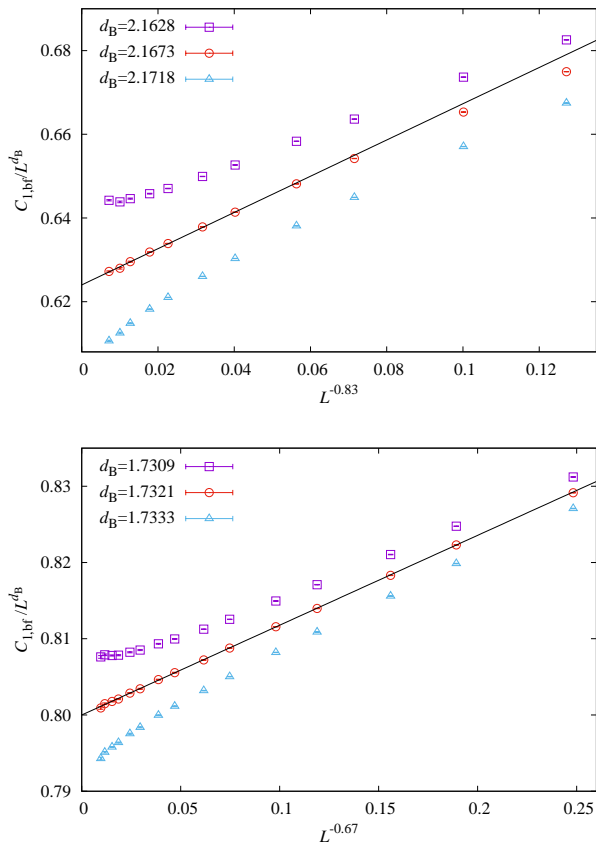


FIG. 7: Plots of $C_{1,bf}/L^{d_B}$ vs $L^{-0.83}$ or vs $L^{-0.67}$ for the critical 3D (top) or 2D (bottom) Ising model, respectively.

with $y_t - d = -1.413$ (3D) and -1 (2D) fixed. For the 3D Ising model, in the fits with y_1 free, we observe that $y_1 \approx -1.2$ for ρ_b , however, for ρ_j and ρ_n , we can not obtain stable fitting results. On this basis, in the subsequent fits we fix $y_1 = -1.2$. For the 2D Ising model, the correction exponent y_1 for ρ_b , ρ_j and ρ_n can not be determined by our MC data when leaving it free. We then try the fits with fixed $y_1 = -1$ or -2 respectively. In both cases, b_1 is found to be consistent with zero. On this basis, we perform the fit with fixed $b_1 = 0$. The fitting results are shown in Table V.

After comparing various fits, we obtain the critical thermodynamic bond densities of various types, including the branch bonds $\rho_{b,0}(3D) = 0.176\,526\,5(1)$ and $\rho_{b,0}(2D) = 0.183\,250\,2(5)$, the junction bonds $\rho_{j,0}(3D) = 0.010\,298\,2(1)$ and $\rho_{j,0}(2D) = 0.023\,856\,2(2)$, as well as the non-bridge bonds $\rho_{n,0}(3D) = 0.051\,342\,35(10)$ and $\rho_{n,0}(2D) = 0.292\,893\,7(9)$. The non-bridge density in 2D is consistent well with the exact result $0.292\,893\,219$ [30, 31]. Among all the occupied bonds, the fraction of the branch, junction and non-bridge bonds are 74.12%, 4.32% and 21.56% for the 3D Ising model, 36.65%, 4.77% and 58.58% for the 2D Ising model, respectively. This suggests that as the spatial dimension d increases, the critical FK clusters become more and more dendritic.

TABLE V: Fits of the bond densities ρ_b , ρ_j and ρ_n for the 3D and 2D Ising models.

	L_{\min}	χ^2/DF	ρ_0	a	b	y_1	
3D	ρ_b	8	6.2/8	0.176 526 50(5)	-0.136 9(1)	0.025(6)	-1.2(2)
		12	4.3/7	0.176 526 47(5)	-0.136 8(1)	0.05(4)	-1.5(3)
		16	3.9/6	0.176 526 49(6)	-0.136 9(2)	0.03(3)	-1.2(5)
		12	5.5/8	0.176 526 50(4)	-0.136 92(5)	0.028(2)	-1.2
		16	3.9/7	0.176 526 49(4)	-0.136 88(6)	0.026(3)	-1.2
		24	3.6/6	0.176 526 48(4)	-0.136 85(8)	0.023(5)	-1.2
	ρ_j	24	6.9/6	0.010 298 17(2)	-0.070 29(3)	0.008(2)	-1.2
		32	5.8/5	0.010 298 18(2)	-0.070 32(4)	0.011(4)	-1.2
		48	4.8/4	0.010 298 19(3)	-0.070 37(8)	0.018(9)	-1.2
	ρ_n	12	5.3/8	0.051 342 34(9)	0.340 1(1)	-0.052(4)	-1.2
		16	4.9/7	0.051 342 35(9)	0.340 1(2)	-0.049(6)	-1.2
		24	4.9/6	0.051 342 35(10)	0.340 1(2)	-0.05(1)	-1.2
2D	ρ_b	24	7.4/9	0.183 250 4(3)	-0.109 68(9)	0.004(3)	-1
		24	6.4/9	0.183 250 3(3)	-0.109 64(6)	0.09(6)	-2
		24	9.6/10	0.183 250 0(3)	-0.109 56(4)	-	-
		32	4.7/9	0.183 250 2(3)	-0.109 60(4)	-	-
	ρ_j	16	8.7/10	0.023 856 2(2)	-0.110 52(4)	-0.0001(8)	-1
		16	8.7/10	0.023 856 2(2)	-0.110 52(3)	0.001(9)	-2
		16	8.7/11	0.023 857 2(2)	-0.110 52(2)	-	-
		24	8.6/10	0.023 856 2(2)	-0.110 52(2)	-	-
	ρ_n	24	7.5/9	0.292 893 6(8)	0.311 4(2)	-0.005(6)	-1
		24	7.0/9	0.292 893 7(7)	0.311 4(1)	-0.1(1)	-2
		24	8.2/10	0.292 894 0(6)	0.311 25(7)	-	-
		32	5.2/9	0.292 893 7(6)	0.311 33(9)	-	-

TABLE VI: Summary of the estimates of the critical exponents and the universal critical wrapping probabilities.

	2D		3D	
	Present	Previous	Present	Previous
$R_c^{(x)}$	-	0.627 138 794 [8]	0.457 5(1)	-
$R_c^{(2)}$	-	0.480 701 867 [8]	0.332 0(2)	-
$R_c^{(3)}$	-	-	0.267 2(2)	-
d_F	1.875 01(5)	15/8 [25, 26]	2.481 8(4)	2.481 6(1) [23]
d_{\min}	1.094 0(3)	1.095 5(10) [27]	1.259 4(2)	-
d_B	1.732 1(4)	1.730 4(3) [29]	2.169 2(15)	2.171(4) [28]

V. SUMMARY AND DISCUSSION

In this work, we investigate the Ising model from the perspective of the geometric properties of the FK clusters. We find that the wrapping probabilities, a kind of topological quantities, suffer less from finite-size corrections near the critical point, and thus they provide a powerful tool for locating the critical point. This leads to a high-precision estimate for the 3D Ising model $K_c = 0.221\,654\,631(8)$, a competing result with the most recent one $0.221\,654\,626(5)$ [4]. The probability distribution is observed to follow a single-variable function $P(C_1, L)dC_1 \equiv \tilde{P}(x)dx$, with $x \equiv C_1/L^{d_F}$. The scaling function $\tilde{P}(x)$ displays a very rich behavior within the scaling window $\Delta \equiv L^{y_t}(K - K_c)$, with a finite constant Δ , including a bimodal feature. We also study other quantities that characterize the geometric ‘‘compactness’’ of the critical FK clusters. In particular, we determine the shortest-path fractal dimension $d_{\min}(3D) = 1.259\,4(2)$ and $d_{\min}(2D) = 1.094\,0(3)$ from the graph distances and the backbone fractal dimension $d_B(3D) = 2.169\,2(15)$ and $d_B(2D) = 1.732\,1(4)$. A brief

summary is given in Table VI.

These results, together with the thermodynamic bond densities of various types, suggest that as the spatial dimension increases, the critical FK clusters become more and more dendritic. The FK representation of the Ising model provides much richer critical behaviors than the spin representation, which are not well understood yet. For instance, even in 2D, it remains to be an open question whether the shortest-path and backbone dimensions take some fractional numbers, and if so, what their values are.

Finally, we note that recent developments of the logarithmic conformal field theory have provided some new insights for non-local geometric correlation functions for the critical Potts model, including the 3D percolation model [32, 33]. Another recent development is the conformal-bootstrap program, which leads to a very high-precision estimate of critical exponents for local operators for the 3D Ising model [34, 35]. Our work might provide a solid numerical test ground for some fantastic theoretical developments in future.

VI. ACKNOWLEDGMENTS

This work was supported by the National Science Fund for Distinguished Young Scholars (NSFDYS) under Grant No. 11625522 (Y.J.D), the National Natural Science Foundation of China (NSFC) under Grant No. 11405039 (J.F.W), the Fundamental Research Fund for the Central Universities under Grant No. J2014HGBZ0124 (J.F.W), and by Anhui University under Start-up Grant No. J01006187 (H.H).

Appendix A: Other quantities

In addition to those in the main text, we have also considered several other quantities in the Monte Carlo simulations, including

- The energy density \mathcal{E} and its square \mathcal{E}^2 , where \mathcal{E} is defined as $\mathcal{E} = \frac{1}{dL^d} \sum_{\langle xy \rangle} \sigma_x \sigma_y$.
- The number of clusters \mathcal{N}_c .
- The second cluster-size moments $\mathcal{S}_2 = \sum_k \mathcal{C}_k^2$, where the sum runs over all the clusters and \mathcal{C}_k denotes the size of the k th cluster.
- An observable $\mathcal{F} := \frac{1}{dL^d} \sum_{k=0}^{d-1} \left| \sum_{\mathbf{x}} \sigma_{\mathbf{x}} \exp(i \frac{2\pi x_k}{L}) \right|^2$, which is the Fourier transform of the correlation function at the lowest nonzero momentum.

We measure the following quantities:

TABLE VII: Fits of $g_{ER}^{(x)}$ for the 3D and 2D Ising models.

	L_{\min}	χ^2/DF	y_t	a_0	b_1	y_1	b_2
3D	12	6.5/8	1.586 7(3)	0.492 2(9)	-0.651(3)	-0.815(5)	-
	16	6.0/7	1.586 5(4)	0.493(2)	-0.648(6)	-0.811(7)	-
	24	4.8/6	1.587 0(6)	0.491(2)	-0.66(2)	-0.82(2)	-
	12	7.4/8	1.587 2(2)	0.490 4(4)	-0.672(3)	-0.83	0.09(3)
	16	5.0/7	1.587 0(2)	0.490 9(5)	-0.677(5)	-0.83	0.15(5)
	24	4.7/6	1.587 2(3)	0.490 6(9)	-0.673(10)	-0.83	0.1(2)
2D	6	7.5/12	0.999 8(8)	0.428(3)	-0.474(2)	-0.456(4)	-
	8	7.4/11	0.999 8(10)	0.428(4)	-0.474(2)	-0.456(6)	-
	12	7.0/10	1.000 5(15)	0.426(5)	-0.473(2)	-0.46(1)	-
	8	7.9/12	1.000 4(2)	0.425 9(3)	-0.472 6(8)	-0.46	-
	12	7.0/11	1.000 3(2)	0.426 2(5)	-0.473(1)	-0.46	-
	16	6.9/10	1.000 2(3)	0.426 3(6)	-0.474(2)	-0.46	-

- The covariance of $\mathcal{R}^{(x)}$ and \mathcal{E}

$$g_{ER}^{(x)} = \langle \mathcal{R}^{(x)} \mathcal{E} \rangle - \langle \mathcal{R}^{(x)} \rangle \langle \mathcal{E} \rangle, \quad (\text{A1})$$

which scales as $g_{ER}^{(x)} \sim L^{y_t}$ at K_c , with $y_t = 1/\nu$ the thermal exponent.

- The cluster number density $\rho = \langle \mathcal{N}_c \rangle / L^d$, whose leading scaling term is proportional to L^{y_t-d} .
- Specific heat $C_e = L^d (\langle \mathcal{E}^2 \rangle - \langle \mathcal{E} \rangle^2)$, which scales as $C_e \sim L^{2y_t-d} = L^{\alpha/\nu}$ at K_c .
- Susceptibility $\chi = \langle \mathcal{S}_2 \rangle / L^d$, which scales as $\chi \sim L^{2d_F-d} = L^{\gamma/\nu}$ at K_c .
- The second moment correlation length

$$\xi_{2nd} = \sqrt{\frac{\chi/F - 1}{4 \sin^2 \pi/L}}, \quad (\text{A2})$$

where $F = \langle \mathcal{F} \rangle$. At K_c , the ratio ξ_{2nd}/L takes an non-zero universal value in the thermodynamic limit $L \rightarrow \infty$.

1. Estimating y_t

We estimate y_t by studying the covariance $g_{ER}^{(x)}$ for the 3D and 2D Ising models at the critical couplings $K = 0.221 654 63$ (3D) and $K_c = 0.440 686 79$ (2D), respectively. The MC data is fitted to Eq. (6) with y_A being replaced by y_t . We note that, in percolation case [13], similar procedure for estimating y_t has been found preferable to methods, such as that employed in [36], in which y_t is estimated by studying how quantities behave in the neighborhood of the percolation threshold.

For the 3D Ising model, in the fit with $b_2 = 0$ fixed and y_1 free, we find $y_1 \approx -0.83$. We then perform the fit with $y_1 = -0.83$ and $y_2 = -2$ fixed. For the 2D Ising model, when leave $b_2 = 0$ fixed and y_1 free, we determine $y_1 \approx -0.46$. The fitting results are shown in Table VII.

After comparing various fits, we estimate the thermal scaling exponent for the 3D and 2D Ising models as $y_t = 1.587 0(5)$ (3D) and $-1.000(1)$ (2D), respectively.

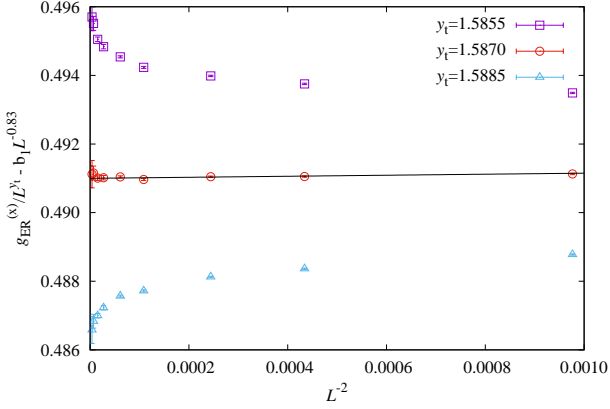


FIG. 8: Plot of $g_{ER}^{(x)}/L^{y_t} - b_1 L^{-0.83}$ versus L^{-2} for the 3D Ising model, using three different values of y_t . The value of b_1 is taken from Table VII.

In order to illustrate our estimate of y_t for the 3D Ising model, we plot $g_{ER}^{(x)}/L^{y_t} - b_1 L^{-0.83}$ versus L^{-2} using three different values of y_t : our estimate, as well as our estimate plus or minus three standard deviations, and show them in Fig. 8. Using the estimated value of y_t should produce a straight line for large L . In the figure, the data using $y_t = 1.5855$ and $y_t = 1.5885$ respectively bend upward and downward, suggesting that the true value of y_t does indeed lie within 3σ of our estimate. The data with $y_t = 1.5870$ appear to be consistent with an asymptotically straight line. For the 2D Ising model, our estimate of y_t is consistent well with the analytical result $y_t = 1$, as expected.

2. Cluster number density ρ

At $K = K_c$ and for $L \rightarrow \infty$, the FK cluster number density shall approach to a non-universal (model-dependent) constant ρ_0 . We fit the MC data of ρ for the 3D and 2D Ising models to Eq.(8). For the 3D Ising model, in the fit with y_t and y_1 free, we observe that $y_t = 1.587(3)$ which is consistent with our estimated $y_t = 1.5870(5)$. On this basis, we further perform the fit with $y_t = 1.587$ fixed and y_1 free, and observe that the correction exponent $y_1 \approx -1.47$. To reduce one fitting parameter, we also try the fit with $y_t = 1.587$ and $y_1 = -1.47$ fixed. For the 2D Ising model, if letting $y_t = 1$ fixed and y_1 free, we observe that the correction exponent $y_1 \approx -1$. To reduce one fitting parameter, we then try the fit with $y_1 = -1$ fixed. The fitting results are shown in Table. VIII. After comparing various fits, we estimate the critical cluster number densities as $\rho_0 = 0.3155882(2)$ (3D) and $0.1286796(6)$ (2D), respectively.

In Fig. 9, we plot $(\rho - \rho_0)L^{d-y_t}$ versus $L^{-1.47}$ (3D) and versus L^{-1} (2D). In both cases, for large system sizes the data points are arranged in a straight line, as expected.

TABLE VIII: Fits of the cluster number density ρ for the 3D and 2D Ising models.

	L_{\min}	χ^2/DF	ρ_0	a	y_t	b	y_1	
3D	12	2.4/7	0.31558826(9)	-0.2820(9)	1.5875(7)	1.04(4)	-1.49(2)	
	16	1.4/6	0.3155882(1)	-0.283(2)	1.587(1)	0.96(9)	-1.45(5)	
	24	1.2/5	0.3155882(2)	-0.282(3)	1.587(2)	1.1(3)	-1.49(12)	
	12	3.0/8	0.31558819(4)	-0.28267(6)	1.587	1.01(2)	-1.470(7)	
	16	1.4/7	0.31558821(5)	-0.28273(7)	1.587	0.98(3)	-1.46(2)	
	12	3.0/9	0.31558819(3)	-0.28267(3)	1.587	1.009(2)	-1.47	
	16	2.5/8	0.31558818(4)	-0.28266(3)	1.587	1.007(3)	-1.47	
	2D	8	10.6/11	0.1286795(3)	-0.0912(1)	1	0.974(3)	-1.002(2)
		12	10.6/10	0.1286794(4)	-0.0912(2)	1	0.974(8)	-1.002(4)
16		7.8/9	0.1286791(4)	-0.0910(2)	1	0.993(14)	-1.009(6)	
8		11.2/12	0.1286796(2)	-0.09129(4)	1	0.9715(5)	-1	
12		10.8/11	0.1286796(3)	-0.09127(5)	1	0.9710(9)	-1	
16		10.3/10	0.1286796(3)	-0.09130(6)	1	0.972(2)	-1	

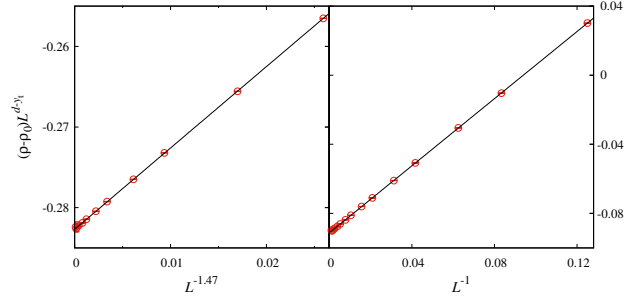


FIG. 9: Plots of the cluster number density $(\rho - \rho_0)L^{1.413}$ versus $L^{-1.47}$ for the 3D (left) Ising model and $(\rho - \rho_0)L$ versus L^{-1} for the 2D (right) Ising model at the critical temperature.

3. Specific heat C_e

According to the scaling theory, specific heat at criticality scales as $C_e \sim L^{\alpha/\nu}$. In order to fit the MC data of C_e , the fitting ansatz Eq.(6) is reformulated by adding a constant term c_0 due to the existence of analytic background, leading to

$$\mathcal{A} = c_0 + L^{y_A}(a_0 + b_1 L^{y_1} + b_2 L^{y_2}), \quad (\text{A3})$$

where the exponent y_A stands for α/ν . For the 3D Ising model, in the fit with $b_2 = 0$ fixed and y_1 free, we observe that $y_1 \approx -1.5$. To reduce one fitting parameter, we perform the subsequent fit with both $y_1 = -1.5$ and $b_2 = 0$ fixed. Besides, we also perform the fit with both $y_1 = -0.83$ and $y_2 = 2y_1 = -1.66$ fixed.

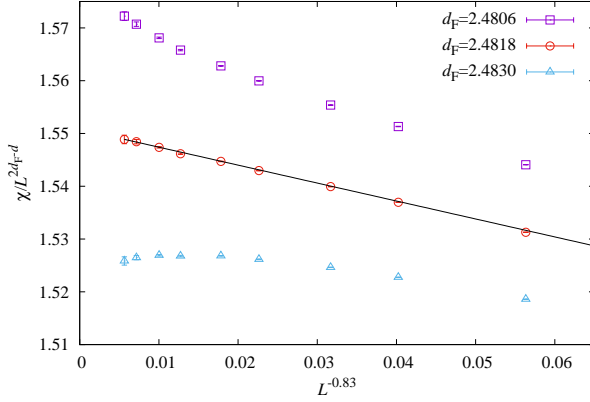
For the 2D Ising model, since $\alpha = 0$, the leading scaling term L^{y_A} changes to $\ln L$. We fit the MC data of C_e to the following equation [37, 38]

$$\mathcal{A} = a_0 \ln L + c_0 + b_1 L^{-1} + b_2 L^{-2}. \quad (\text{A4})$$

In the fitting results b_2 is consistent with zero. On this basis, we perform the fit with $b_2 = 0$ fixed. The fitting results are reported in Table IX. For 2D Ising model, $a_0 = 0.6366(5)$ is consistent with the theoretical value $a_0 = 2/\pi$ [38].

TABLE IX: Fits of C_e for the 3D and 2D Ising models.

	L_{\min}	χ^2/DF	α/ν	c_0	a_0	b_1	y_1	b_2	
3D	8	7.1/8	0.169(1)	-3.61(7)	4.83(6)	-1.76(10)	-1.49(6)	-	
	12	7.0/7	0.170(2)	-3.6(2)	4.8(1)	-1.7(3)	-1.4(2)	-	
	16	4.5/6	0.174(5)	-3.3(4)	4.6(3)	-1.0(3)	-1.1(3)	-	
	12	7.2/8	0.169 3(6)	-3.62(4)	4.84(3)	-1.77(4)	-1.5	-	
	16	7.0/7	0.169 1(7)	-3.63(5)	4.85(4)	-1.74(8)	-1.5	-	
	24	4.7/6	0.170(2)	-3.54(8)	4.78(6)	-2.0(2)	-1.5	-	
	8	6.7/8	0.171(2)	-3.5(1)	4.73(8)	-0.24(8)	-0.83	-1.7(2)	
	12	6.7/7	0.171(3)	-3.4(2)	4.7(2)	-0.3(2)	-0.83	-1.7(4)	
	2D	6	10.7/12	-	0.178(2)	0.6365(4)	-0.22(2)	-1	0.05(6)
		8	10.1/11	-	0.180(3)	0.6363(5)	-0.24(3)	-1	0.1(2)
6		11.3/13	-	0.1772(9)	0.6367(2)	-0.211(4)	-1	-	
8		11.2/12	-	0.1774(1)	0.6367(3)	-0.212(6)	-1	-	
12		10.3/11	-	0.1785(2)	0.6365(4)	-0.22(1)	-1	-	

FIG. 10: Plots of χ vs $L^{-0.83}$ at K_c for the 3D Ising model.

4. Susceptibility χ

We fit the MC data of χ in 3D and 2D to Eq.(6) with the exponent y_A replaced by $2d_F - d$. For the 3D Ising model, in the fit with $y_2 = -2$ fixed and y_1 free, we observe that $y_1 \approx -0.83$. To reduce one fitting parameter, in the subsequent fit we fix $y_1 = -0.83$ and $y_2 = -2$. For the 2D Ising model, when leave $b_2 = 0$ fixed and y_1 free, we determine $y_1 \approx -2$. On this basis, we perform the fit with $y_1 = -2$ and $b_2 = 0$ fixed. The fitting results are shown in Table X.

From these fits, we get the estimate $d_F = 2.4818(4)$ (3D) and $d_F = 1.87500(4)$ (2D), respectively. In Fig. 10, we plot χ/L^{2d_F-d} versus $L^{-0.83}$ using three different values of d_F for the 3D Ising model: our estimate, as well as our estimate plus or minus three standard deviations. As L increases, the data with $d_F = 2.4806$ and $d_F = 2.4830$ bend upward and downward, respectively, while the data with $d_F = 2.4818$ are consistent with an asymptotically straight line.

5. The second moment correlation length ξ_{2nd}

At $K = K_c$, the ratio ξ_{2nd}/L approaches a universal value $(\xi_{2nd}/L)_c$ in the thermodynamic limit $L \rightarrow \infty$. It

TABLE X: Fits of χ for the 3D and 2D Ising models.

	L_{\min}	χ^2/DF	d_F	a_0	b_1	y_1	b_2
3D	8	5.6/8	2.481 77(16)	1.551(2)	-0.30(2)	-0.80(4)	-0.86(8)
	12	5.5/7	2.481 7(3)	1.552(3)	-0.29(5)	-0.78(8)	-0.9(2)
	8	6.2/9	2.481 88(3)	1.549 1(5)	-0.319(3)	-0.83	-0.79(2)
	12	5.9/8	2.481 86(5)	1.549 2(8)	-0.321(6)	-0.83	-0.77(5)
	16	4.8/7	2.481 82(7)	1.550(1)	-0.329(9)	-0.83	-0.7(1)
2D	8	12.8/11	1.875 00(2)	1.092 1(2)	-0.14(2)	-1.71(7)	-
	12	12.7/10	1.875 00(2)	1.092 0(2)	-0.16(6)	-1.8(2)	-
	16	10.4/10	1.875 007(10)	1.091 9(1)	-0.30(2)	-2	-
	24	10.4/9	1.875 007(13)	1.091 9(2)	-0.30(4)	-2	-
	32	7.0/8	1.875 02(2)	1.091 7(2)	-0.17(8)	-2	-

TABLE XI: Fits of ξ_{2nd} for the 3D and 2D Ising models.

	L_{\min}	χ^2/DF	$(\xi_{2nd}/L)_c$	b_1	y_1	b_2
3D	12	10/8	0.64321(9)	-0.026(4)	-0.72(6)	0.02(3)
	16	7.3/7	0.64310(10)	-0.037(10)	-0.83(9)	0.11(7)
	16	7.4/8	0.64310(3)	-0.0367(8)	-0.83	0.11(2)
	24	7.1/7	0.64309(4)	-0.036(1)	-0.83	0.09(5)
	32	6.9/6	0.64310(5)	-0.037(2)	-0.83	0.13(9)
2D	8	6.4/12	0.905 05(6)	0.46(2)	-1.54(2)	-
	12	6.3/11	0.905 06(7)	0.48(4)	-1.56(4)	-
	16	6.2/10	0.905 06(8)	0.47(7)	-1.55(6)	-
	8	6.5/13	0.905 06(4)	0.468(2)	-1.55	-
	12	6.3/12	0.905 05(4)	0.469(4)	-1.55	-
16	6.2/11	0.905 06(5)	0.468(7)	-1.55	-	

means that the second moment correlation length scales as $\xi_{2nd} \sim L$. We fit the MC data of ξ_{2nd} for the 3D and 2D Ising models to Eq.(6) with $y_A = 1$ fixed and a_0 replaced by $(\xi_{2nd}/L)_c$. For the 3D Ising model, in the fit with $y_2 = -2$ fixed and y_1 free, we observe that the correction exponent $y_1 \approx -0.83$. To reduce one fitting parameter, we further perform the fit with $y_1 = -0.83$ and $y_2 = -2$ fixed. For the 2D Ising model, if letting $b_2 = 0$ and y_1 free, we observe that the correction exponent $y_1 \approx -1.55$. To reduce one fitting parameter, we then try the fit with fixed $y_1 = -1.55$. The fitting results are shown in Table XI.

After comparing these fits, we determine the universal critical ratio as $(\xi_{2nd}/L)_c = 0.6431(1)$ (3D) and $0.90506(8)$ (2D), respectively. The current estimates for the 3D and 2D Ising models agree well with the previous reported value $(\xi_{2nd}/L)_c(3D) = 0.6431(1)$ [24], and the numerical integration result $(\xi_{2nd}/L)_c(2D) = 0.9050488292(4)$ [39] using conformal field theory, respectively.

[1] E. Ising, Z. Phys. **31**, 253 (1925).[2] L. Onsager, Phys. Rev. **64**, 117 (1944).

[3] R. J. Baxter, Exactly Solved Models in Statistical Me-

chanics (Academic Press, 1982).

[4] A. M. Ferrenberg, J. Xu and D. P. Landau, Phys. Rev. E **97**, 043301 (2018).

- [5] P. W. Kasteleyn and C. M. Fortuin, *J. Phys. Soc. Jpn.* **26** (Suppl.), 11 (1969); C. M. Fortuin and P. W. Kasteleyn *Physica (Amsterdam)* **57**, 536 (1972).
- [6] R. H. Swendsen and J. S. Wang, *Phys. Rev. Lett.* **58**, 86 (1987).
- [7] R. G. Edwards and A. S. Sokal, *Phys. Rev. D* **38**, 2009 (1988).
- [8] R. P. Langlands, C. Pichet, P. Pouliot and Y. Saint-Aubin, *J. Stat. Phys.* **67**, 553 (1992).
- [9] H. T. Pinson, *J. Stat. Phys.* **75**, 1167 (1994).
- [10] L. P. Arguin, *J. Stat. Phys.* **109**, 301 (2002).
- [11] R. M. Ziff, C. D. Lorenz and P. Kleban, *Physica A* **266**, 17 (1999).
- [12] M. E. J. Newman and R. M. Ziff, *Phys. Rev. E* **64**, 016706 (2001).
- [13] J. Wang, Z. Zhou, W. Zhang, T. M. Garoni, and Y. Deng, *Phys. Rev. E* **87**, 052107 (2013).
- [14] U. Wolff, *Phys. Rev. Lett.* **62**, 361 (1989).
- [15] X. Xu, J. F. Wang, Z. Zhou, T. M. Garoni, Y. Deng, *Phys. Rev. E* **89**, 012120 (2014).
- [16] W. Huang, P. C. Hou, J. F. Wang, R. M. Ziff and Y. J. Deng, *Phys. Rev. E* **97**, 022107 (2018).
- [17] E. P. Münger and M. A. Novotny, *Phys. Rev. B* **43**, 5773 (1991).
- [18] B. Nienhuis, *J. Stat. Phys.* **34**, 731 (1984).
- [19] P. di Francesco, H. Saleur and J. B. Zuber, *J. Stat. Phys.* **49**, 57 (1987).
- [20] J. L. Cardy, *J. Phys. A: Math. Gen.* **25**, L201 (1992).
- [21] H. Hu and Y. Deng, *Nucl. Phys. B.* **898**, 157 (2015).
- [22] P. H. L. Martins and J. A. Plascak, *Phys. Rev. E* **67**, 046119 (2003).
- [23] Y. Deng and H. W. J. Blöte, *Phys. Rev. E* **68**, 036125 (2003).
- [24] M. Hasenbusch, *Phys. Rev. B* **82**, 174433 (2010).
- [25] C. N. Yang, *Phys. Rev.* **85**, 808 (1952).
- [26] B. Nienhuis, in *Phase Transitions and Critical Phenomena*, edited by C. Domb and J. L. Lebowitz (Academic Press, New York, 1987), Vol. **11**.
- [27] Y. Deng, W. Zhang, T. M. Garoni, A. D. Sokal and A. Sportiello, *Phys. Rev. E* **81**, 020102 (2010).
- [28] Y. Deng and H. W. J. Blöte, *Phys. Rev. E* **70**, 046106 (2004).
- [29] Y. Deng, H. W. J. Blöte and B. Nienhuis, *Phys. Rev. E* **69**, 026114 (2004).
- [30] E. M. Elci, M. Weigel, N. G. Fytas, *Nucl. Phys. B* **903**, 19 (2016).
- [31] H. Hu, H. W. J. Blöte, R. M. Ziff, Y. Deng, *Phys. Rev. E* **90**, 042106 (2014).
- [32] X. J. Tan, R. Couvreur, Y. J. Deng and J. L. Jacobsen, arXiv:1809.06650 (2018).
- [33] R. Couvreur, J. L. Jacobsen and R. Vasseur, *J. Phys. A: Math. Theor.* **50**, 474001 (2017).
- [34] S. El-Showk, M. F. Paulos, S. Rychkov, D. Simmons-Duffin and A. Vichi, *Phys. Rev. D* **86**, 025022 (2012).
- [35] D. Poland, S. Rychkov and A. Vichi, arXiv:1805.04405 (2018).
- [36] Y. Deng and H. W. J. Blöte, *Phys. Rev. E* **72**, 016126 (2005).
- [37] A. E. Ferdinand and M. E. Fisher, *Phys. Rev.* **185**, 832 (1969).
- [38] J. Salas, *J. Phys. A: Math. Gen.* **34**, 1311 (2001).
- [39] J. Salas and A. D. Sokal, *J. Statist. Phys.* **98**, 551 (2000).